Implementation of Liquid Crystal Thermography to Determine Wall Temperatures and Heat Transfer Coefficients in a Tube-in-Tube Heat Exchanger

Jacob E. van der Westhuizen, Jaco Dirker* and Josua P. Meyer

Department of Mechanical and Aeronautical Engineering, University of Pretoria, Pretoria, South Africa

*Corresponding Author: jaco.dirker@up.ac.za, +27 12 420 2465

Abstract

Liquid crystal thermography was used in a water-operated concentric tube-in-tube heat exchanger to determine local annular heat transfer coefficients at the inlet region. An annular diameter ratio of 0.54 was considered with the inlet and outlet orientated perpendicularly to the axial flow direction. Both heated and cooled cases were considered at annular Reynolds numbers ranging from 1000 to 13 800. Wall temperature distributions were directly measured by means of a coating of thermo-chromic liquid crystals. Local heat transfer coefficients at the inlet were higher than those predicted by most correlations, but good agreement was obtained with some literature.

Keywords: Liquid Crystal Thermography, Experimental method, Heat transfer coefficients, Developing inlet region

1. Introduction

Tube-in-tube heat exchangers are commonly found in industry as they are relatively inexpensive to manufacture and easy to maintain. It is therefore essential that the performance and heat transfer ability of this type heat exchanger are understood in order to design them effectively. Several investigations have been conducted to obtain friction factor and heat transfer data for the annular space in tube-in-tube heat exchangers. Table 1 gives a selection of available annular heat transfer coefficients correlations [1-4] which takes into consideration, for instance, the annular diameter ratio and other geometric and thermo-physical parameters. It has been reported, however, that often these correlations and others produce conflicting predictions [1, 5] and that differences of up to 20 % have been found to exist. These discrepancies may also be expected for other types of heat exchangers such as rectangular channels and parallel plates [6], but in this paper we consider annular spaces only.

Generally, correlations such as those presented in Table 1 do not specifically take into consideration the inlet and developing regions of heat exchangers. In most cases of turbulent flow it is assumed that fully developed flow occurs within 10 hydraulic diameters and that this part is negligible when the total length is taken into consideration. Total or average heat transfer coefficients are usually considered while localized results are often disregarded, left unpublished or not investigated. Some correlations such as the one by Gnielinski [3] do make provision for the impact of the relative heat exchanger length. This is because high heat transfer rates in the inlet regions may be dominant in terms of the relative flow development length (related to the fluid's Prandtl number) compared to the total heat exchanger length.

Table 1 Some existing correlations in literature.

Author	Correlation	α	Re	Medium
Dirker and Meyer [1]	$Nu_h = C_o Re_h^P Pr^{1/3} \left(\frac{\mu_o}{\mu_{o,w}}\right)^{0.14}$ $P = 1.013e^{-0.0067/a}$ $C = (0.003a^{-1.86})/(0.063a^{-3} - 0.0674a^{-2} + 2.225/a - 1.157)$	0.3125-0.588	4000-30000	Water
Dittus and Boelter [2]	$Nu_h = 0.023Re_h^{0.8}Pr^m$, $m = 0.4$ for heating $m = 0.3$ for cooling	Not specified	Not specified	Not specified
Gnielinski [3]	$Nu_h = \frac{\left(\frac{f}{8}\right)Re_h Pr_o}{G_1 + 12.7\sqrt{\frac{f}{8}}\left(Pr_o^{\frac{2}{3}} - 1\right)}\left(1 + \left(\frac{D_h}{L}\right)^{\frac{2}{3}}\right)G_2 G_3$ $G_1 = 1.07 + \frac{900}{Re_h} - \frac{0.63}{1+10Pr_o}$, $G_2 = \left(\frac{Pr_o}{Pr_{iw}}\right)^{0.11}$ for liquids $G_2 = \left(\frac{T_b}{T_{iw}}\right)^m$ for gasses and $m = 0$ for cooling $m = 0.45$ with $0.5 < \frac{T_b}{T_{iw}} < 1.0$ $G_3 = 0.75a^{-0.17}$, $f = (1.8\,log_{10}\,Re^* - 1.5)^{-2}$ $Re^* = Re_h \frac{(1+a^2)\ln a + (1-a^2)}{(1-a)^2 \ln a}$	Not specified	Not specified	All
McAdams [4]	$Nu_h =$ $0.03105a^{-0.15}\,(1/a - 1)^{0.2} Re_h^{0.8} Pr^{1/3}\,\left(\frac{\mu}{\mu_w}\right)_o^{0.14}$	0.00014-0.84	Not specified	All

In a recent study of tube-in-tube heat exchangers operated with water in the turbulent flow regime with inlet and outlet ports that were perpendicular to the axial flow [7], it was found that based on the value of the local heat transfer coefficient the flow seldom became thermally fully developed even for relatively long heat exchangers (with length to diameter ratios between 280 and 715). It was shown that the local heat transfer coefficients closer

towards the inlet were significantly higher than the averaged measured heat transfer coefficients. The heat transfer coefficients asymptotically approached a constant value downstream from the inlet.

This trend is also covered in Cengel's book [8] where it is shown that the heat transfer capability increases with a logarithmic form towards the inlet of the heat exchanger. Experimental and numerical studies that report on this include those by Maranzana *et al.* [9] and Mirzael *et al.* [10] for mini and micro channels, and theoretically in the laminar flow regime by Singh [11] and Shiniyan *et al.* [12]. Different inlet configurations have also been reported to influence the heat transfer. For instance, Ghajar and Tam [13] investigated re-entrant, square-edged and bell-mouth inlets for a circular tube and observed different transitional flow behaviour.

The higher heat transfer coefficients closer to the inlet are generally due to high levels of flow mixing due to geometrical conditions (such as a 90° elbow inlet) and the subsequent break-down of the thermal boundary layer. The flow only starts to develop along the length of the heat exchanger resulting in a thicker boundary layer that traps slower moving fluid particles close to the surface of the heat exchange wall. This causes heat to be transferred via conduction, which is significantly weaker when compared to convection.

Since the length of a tube-in-tube heat exchanger can significantly influence the average measured heat transfer coefficient, and since it is often not known for what length a particular heat transfer correlation was developed, additional investigations into the local heat transfer coefficient, especially close to the inlet, is needed. However, to obtain accurate local heat transfer characteristics, local heat transfer wall temperatures and bulk fluid temperatures are to be measured in a reliable fashion. This poses a practical problem,

especially when the experimental technique relies on intrusive measurement techniques such as the use of thermocouples. The electrical leads of thermocouples may, for instance, alter the flow field in an otherwise empty flow channel.

A possible alternative to the use of thermocouples are Liquid Crystal Thermography (LCT) which is a non-intrusive temperature measurement technique which utilises Thermo-chromic Liquid Crystals (TLC) and is not reliant on electrical leads at the measuring location. TLC's change their reflected colour in the presence of white light according to the crystal temperature [14-16]. It has been used to obtain wall temperature profiles by applying it to heat transfer surfaces [17-19] or for determining local fluid temperatures by suspending TLC-treated particles within fluids [20-22].

By treating a heat exchange surface, for instance the inner annular wall of a tube-in-tube heat exchanger, with TLC impregnated paint, it should be possible to obtain a complete surface temperature map of a particular region under investigation as long as it is visually accessible. By investigating these temperature maps, it should be possible to identify regions with increased or decreased heat transfer coefficients.

Therefore, the advantage of using LCT is the high density of the temperature sample points that van be obtained; from which temperature maps may be constructed. This is in strong contrast to the discreet temperature measurements provided by thermocouples. When observing temperature maps generated by the method used in the current study, it is clear that even with a material with a high thermal conduction value, such as copper, the temperature gradients present on the surface can vary considerably. It will not always be possible to fully capture the average surface temperature accurately by placing only a few thermocouples around the circumference at a given axial position of a heat exchanger test

section, especially in the inlet region. In addition, wall temperature measurement using embedded thermocouples are troublesome and practically difficult to achieve.

The purpose of this study is to investigate the feasibility of using LCT as primary surface temperature measurement technique on the inner wall of the annulus at the inlet region of a tube-in-tube heat exchanger. Of interest is the usage of obtained temperatures to calculate local annular heat transfer coefficients where it might be impractical to use traditional temperature measurement techniques.

2. Experimental facility

Figure 1 shows the layout of the experimental test facility. The facility featured two distinct flow loops, one for hot water and the other for cold water. To accommodate testing of either a heated or a cooled annulus, any of the two flow loops could be connected to either the annulus or the inner tube of the heat exchanger.

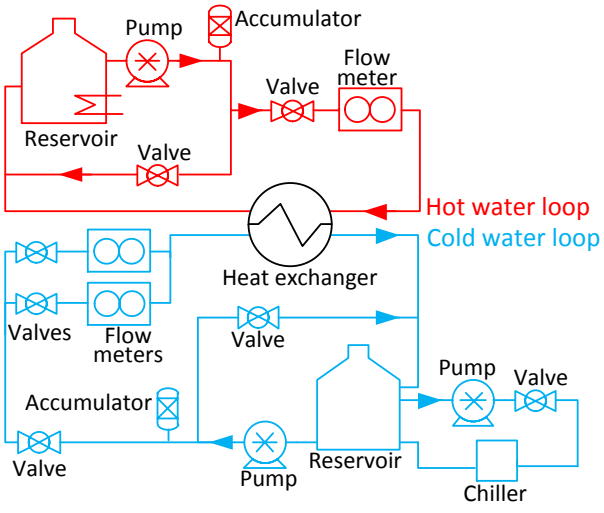

Figure 1 Experimental facility.

Both the hot water and the cold water loops were closed systems. The hot water was extracted from the top of a 600 litre hot water storage tank with a built-in resistance heater (12 kW heating capacity) via a positive displacement pump. After the pump there was a 4 litre accumulator to reduce flow fluctuations. Water could be returned to the geyser directly via a bypass line, and/ or it could be supplied to the test line. Both lines were equipped with hand-controlled valves with which the relative flow rates could be adjusted if needed. The test line contained a Coriolis flow meter which had a capacity of 54.5-1090 *l*/h. Similarly, the cold water loop had a 1000 litre reservoir which was cooled by means of an external chiller which had a 16 kW cooling capacity. Cold water was extracted from the bottom of the reservoir by means of a positive displacement pump. Cold water could be returned to the reservoir directly via a bypass line and/ or it could be directed to the test line. Hand-operated valves were used to adjust the flows if needed. The test line was equipped with a 4 litre accumulator and two parallel connected Coriolis flow meters with flow capacities of 54.5 – 1090 *l*/h and 4.1 – 82 *l*/h respectively. Flow meters selection was made by means of hand valves depending on the prevailing flow rate. After the water passed though the test section, the water was returned to the cold water reservoir.

2.1. Test section

Figure 2 shows a schematic representation of the counter-flow tube-in-tube heat exchanger test section.

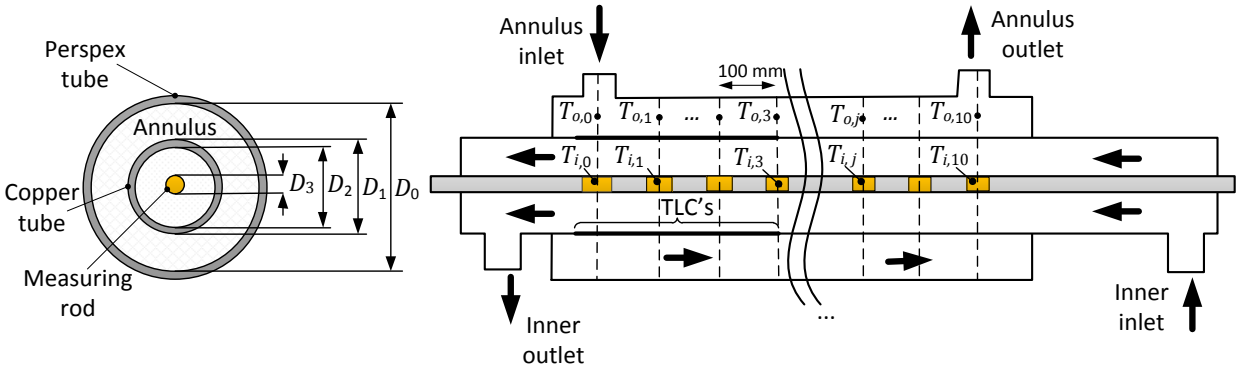

Figure 2 Schematic layout of the test section.

A transparent Perspex tube which had an inner diameter of D_0 = 36.00 mm formed the outer wall of the annulus. The inner wall of the annulus was formed by a copper tube which was held concentrically within the Perspex tube by means of clamps on either side of the heat exchanger. This tube, which had an effective outer diameter of D_1 = 19.47 mm was coated with a thin layer of TLC's for an axial length of approximately 300 mm (measured from the inlet of the annulus). A protective resin layer was also added that covered the entire heat exchanger length. The annular inlet and outlet ports (each consisting of a short acrylic tube section with an inner diameter of 16 mm) were orientated radially at 90° to the axial direction. The test section had a heat transfer length of 1001 mm and the inlet and outlet ports were spaced 945 mm apart (centre-to-centre). Based on this distance between the ports and the hydraulic diameter of $D_{h,o} = D_0 - D_1$= 16.53 mm, this resulted in a length to hydraulic diameter ratio of approximately 57.

The transparent outer wall of the annulus allowed for visual observation and digital recording of the inner annular wall. However, to reduce heat loss from the outer annular wall to the laboratory, thermal insulation was placed around the heat exchanger and

temporary removed at the appropriate axial position to allow for digital recording of the surface temperature profile.

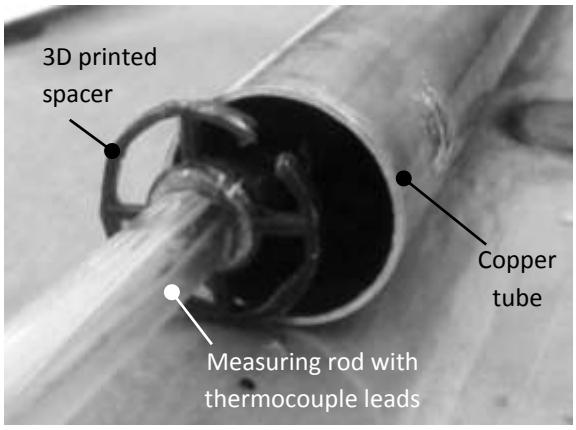

Figure 3 - Photograph of the measuring rod spacer.

In order to measure the local bulk fluid temperature inside the copper tube, a measuring rod with an outer diameter of D_3 = 6.5 mm was placed inside the copper tube and were kept concentric by means of spacers (Figure 3). The rod contained 11 equally spaced (100 mm apart) thermocouple measuring stations (j = 0 to 10) along the length of the heat exchanger. Each measuring station consisted of a copper tube section (with a 5 mm exposed length) with two internally soldered T-type thermocouples as is shown in Figure 4. To prevent axial heat conduction between the measuring stations, they were separated by acrylic tube sections (each 95 mm in length). This also allowed the thermocouple leads to be passed internally to the ends of the test section and prevented the inner flow profile to be disturbed. It was ensured that the measuring rod was fully sealed so that no liquid leakage into it was possible. To improve bulk fluid profile measurement, the inner fluid was allowed to become hydro-dynamically fully developed before entering the heat transfer section by using an extended development length so that the inner fluid velocity profile at each measuring station was the same.

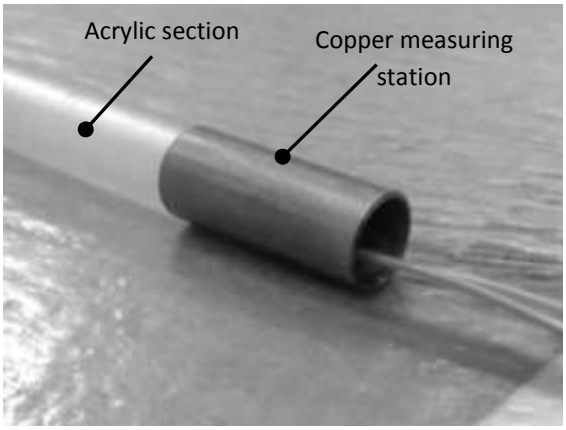

Figure 4 Photograph of thermocouple measuring station.

Besides the thermocouples that were used in the measuring rod, thermocouples were also used to measure the inlet and outlet bulk temperatures of both the annular and inner fluids. For each of these positions a measuring station was created which consisted each of a short copper tube and four T-type thermocouples soldered to its outside. These stations were placed before and after the heat exchanger, but were separated from it via flexible rubber hoses to prevent axial heat conduction. The exit measuring stations were preceded by 90° elbow mixing sections. The measuring stations were also thermally insulated to reduce heat loss or gain from the surroundings. All thermocouples used in this study as well as the TLC's were calibrated against a Pt100 with a manufacturer specified uncertainty of 0.01°C. A third order regression fit was used to correct raw thermocouple data into calibrated thermocouple data.

As mentioned earlier, the outer surface of the copper tube consisted of more than one material layer. Firstly, the tube was coated with a thin layer of black paint having a thickness of less than 0.05 mm which provided the necessary contrast needed to effectively observe the reflected colour from the TLC's. Next there was a TLC layer which had a thickness of less than 0.05mm. The TLC's used in this investigation was obtained from LCR Hallcrest

(SPN300 R20C18W) and had a red start temperature of 20 °C and a band width of 18 °C (making the effective working temperatures between 20 °C and 38 °C) with a value scatter of 0.22 °C. Finally the tube was coated with a protective transparent resin layer spanning its entire length which had a thickness of t_{resin} = 0.20 mm and a thermal conductivity of 0.218 W/mK. In order to obtain repeatable, consistent and uniform thickness of the paint and TLC layer, a custom computer numerically controlled (CNC) painting facility was used which had precise control over the rotation of the copper tube as well as the axial position of a sprayer head. The resin layer was applied as a wet layup and after curing it was sanded down to the correct diameter and a smooth outer surface finish.

A 7 megapixel digital camera was used to record the surface images of the inner annular wall. Figure 5 shows the setup that was employed to concentrically position the camera and the light source around the test section. This positioning system was partly computer controlled which allowed for accurate and repeatable rotation of the mounted camera around the heat exchanger. Axial movement along the length of the heat exchanger was done manually. The light source consisted of six intensity controllable light emitting diodes with a colour temperature of 5500 K which was held in a fixed position relative to the camera.

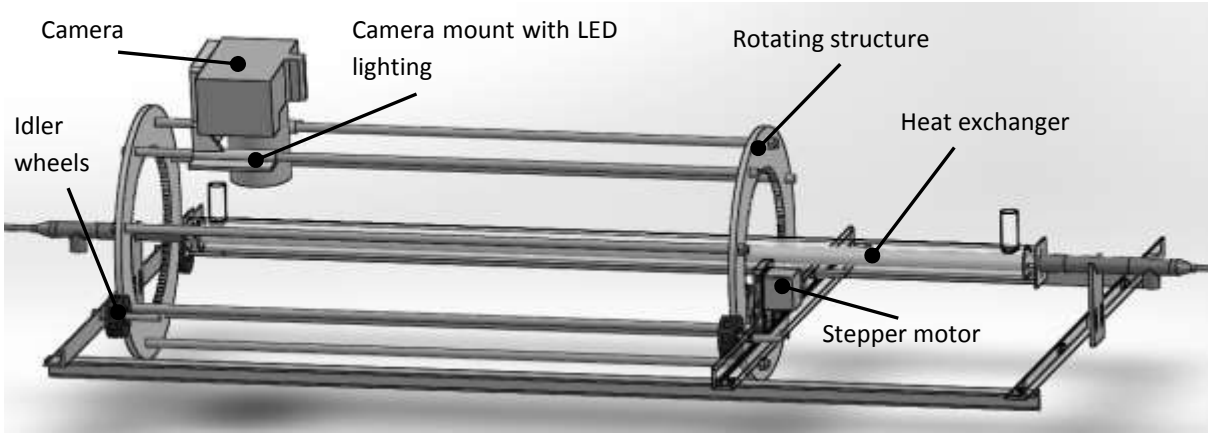

Figure 5 Camera positioning setup.

Data from the thermocouples, and the Coriolis flow meters were collected by a computerised data acquisition (DAQ) system. The DAQ system consisted of a desktop computer on which was installed a LabVIEW program written to automatically acquire needed data, an analogue/digital interface card, shielded cable assembly, signal-conditioning extensions for instrumentation (SCXI), transducer multiplexers, terminal blocks, channel multiplexers and termination units. The program displayed all measurements, including both primary and secondary quantities, which were monitored.

3. Calibration of the TLC treated surface

In order to obtain a relationship between the colour of the reflected light from the TLC treated surface and the corresponding temperature of the surface, the surface reflection was calibrated for a temperature range of 21°C to 38°C. This was done at adiabatic conditions by circulating temperature-controlled water through both the inner flow passage as well as the annular flow passage simultaneously so that no heat was transferred across the inner wall of the annulus. The inlet and outlet temperatures were monitored by means of the previously mentioned PT100's to ensure that the entire heat exchanger was at the same temperature. When steady state conditions were reached for a particular

temperature setting, digital images at different positions were recorded along the length and circumference of the annular inner wall. Since the perceived colour of TLC's are influenced by the incident light [23], all calibrations were conducted at night time while all external light sources were removed except for the light source on the test set-up.

The images were processed by converting them from the RGB (Red Green Blue) colour coordinate system to the HSV (Hue, Saturation, Value) colour coordinate system [24]. The hue value, which is representative of the colour, is not influenced by the brightness or the saturation of the pixels [14]. Thus, by using this as the colour interpretation technique and controlling the light source carefully, ensured consistent and repeatable temperature measurements.

The average hue value for each image set (for a particular temperature setting) was determined. A ±0.22°C scatter was observed over the TLC covered surface, as per the manufacturer specification. Repeatability was checked by performing the calibration several times before and after the experimental investigation. The obtained relationship between the normalized hue values (0 to 1) and temperature is shown in Figure 6. It can be seen that a repeatable calibration profile was achieved. To facilitate data reduction, a sixth order polynomial fit was used to describe the temperature-hue relationship, and the accuracy there-off was incorporated into an uncertainty analysis that is covered later in this paper.

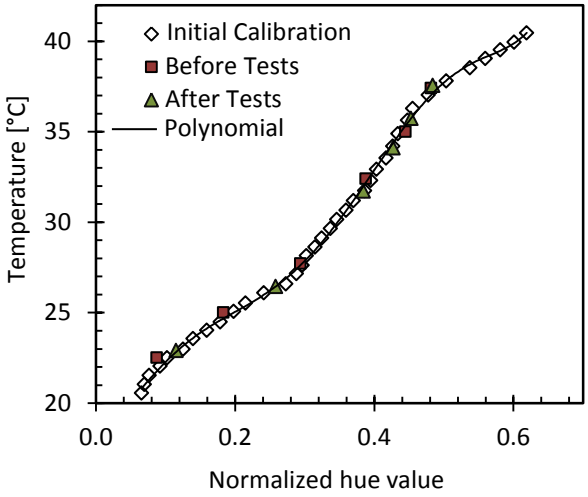

Figure 6 Calibration data for the TLC's.

Table 2 Test cases.

	Cooled annular cases					Heated annular cases			
	CA 1	CA 2	CA 3	CA 4	CA 5	HA 1	HA 2	HA 3	HA 4
Re_o (-)	1000	2500	5000	10 000	13 800	1000	2500	5000	8000
$T_{o,in}$ (°C)	41.8±0.1	42.9±0.3	43.5±0.1	42.7±0.3	43.4±0.7	20.8±0.1	20.5±0.1	20.5±0.2	20.2±0.2
Re_i (-)	3600	3600	3600	3600	3600	3700	3700	3700	3700
$T_{i,in}$ (°C)	21.2±0.1	21±0.1	20.7±0.1	20.6±0.2	20.3±0.1	41.1±0.1	41.6±0.1	41.8±0.1	41.8±0.1

4. Experimental procedure

In order to investigate different thermal conditions, the tests were conducted at a variety of inlet temperature combinations and flow rates for both heated and cooled annular cases. The different test configurations are outlined in Table 2 which shows the applicable inlet temperatures and Reynolds numbers for the cooled cases (CA 1 to CA 5) with an annular inlet temperature of approximately 42 - 44°C and the heated cases (HA 1 to HA 4) with an annular inlet temperature of approximately 20 - 21°C. The temperature variations that are

supplied in this table refer to the variation of the logged inlet temperatures for the duration of each test. Annular Reynolds numbers were specifically chosen to cover both laminar and turbulent flow regimes. The selection of the annular and inner fluid flow rates and inlet temperatures combinations where done carefully to ensure that the inner annular wall temperature fell within the appropriate TLC temperature range. An inner Reynolds number, based on the hydraulic diameter of the inner flow passage, of $\mathrm{Re}_i \approx 3\,700$ was used for all the cases. This chosen flow rate was sufficiently high to ensure mixed turbulent fluid behaviour for the inner bulk fluid temperature monitored via the measuring rod, but also low enough to ensure large enough temperature differences between adjacent thermocouple measuring stations, to reduce such measuring uncertainties.

After setting-up the appropriate mass flow rates and inlet temperatures, testing could be initiated as soon as steady state was reached. For each test case it took approximately 14 minutes to record the full temperature profile on the inner annular wall. Practically it was difficult to maintain strict system steady state conditions for such a length of time. To overcome this, data were captured in parts during quasi steady state conditions, defined as when the inlet to outlet temperature difference (for the inner and the annular fluid respectively) did not change by more than 0.2°C over a period of 2 minutes. For this purpose, the wall temperature profiles were recorded by the camera in seven sub-sets spaced axially at 40 mm intervals along the treated length of the copper tube. Each subset was obtained from one rotation of the camera and are referred to in this paper as rings $n = 1$ to 7.

Once quasi steady state was reached, the appropriate portion of the external thermal insulation was removed to reveal the outer Perspex tube of the heat exchanger such that

image capturing could be initiated. For each data subset, the camera was manually moved to the correct axial position where-after the camera's angular position around the heat exchanger was computer-controlled. For quality control purposes, each image was recorded twice. After each ring was completed, the thermal insulation was replaced. The process was repeated until all the rings were recorded. All thermocouple data was logged continually for data analysis purposes. Full experimental test run cases were also repeated to check for overall repeatability.

5. Data reduction

5.1. Inner annular wall thermography

Based on the camera positioning system, the circumference of the inner wall could be covered by up to 40 image slices, each spanning 9° representing a surface circumferential length of approximately 1.5 mm. Each image also covered an axial length of 40 mm. From this, composite images could be created as shown in Figure 7, given for an arbitrary example case. In this figure darker shading represents warmer spots. By repeating this for all seven axial rings (n = 1 to 7) produced 280 images which could be stitched together to produce a composite image of the tube surface roughly 300 mm long by 61 mm circumferentially.

It was, however, found that 10 equally spaced circumferential images, at 36° intervals or 6.1 mm on the inner wall surface, were sufficient to represent the average local circumferential surface temperature at a particular axial position. The reduction of the number of circumferential images from 40 to 10 resulted in a difference of less than 0.04°C on the calculated average surface temperature.

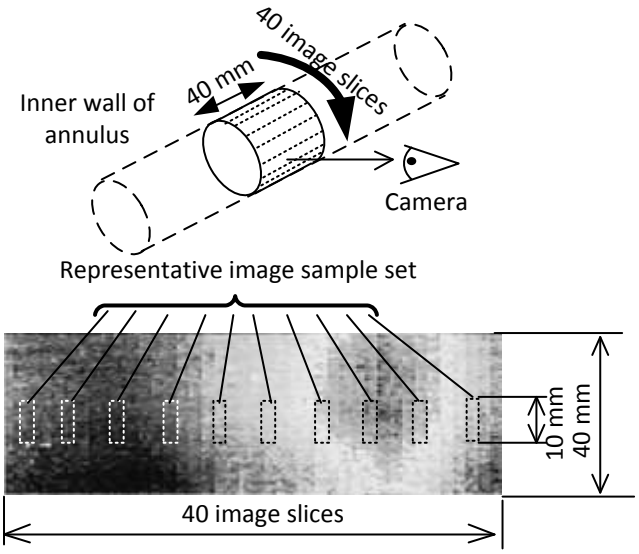

Figure 7 Composite temperature image (darker means warmer).

In order to ensure that the incident and reflected angles of the light was held below 2° relative to the pipe surface (since this could affect the observed colour [25]), only an axial length of 10 mm of each image slice was used. Figure 7 indicates the relative size of the resulting ten sample areas that were used in this study. The number of images in the sample can easily be increased; however, this will result in longer testing times which may impact on the quality of the steady-state conditions. By using the TLC calibration curve, the local temperature field, $T_{TLC}(\phi, x)$ was obtained based on the hue values of pixel clusters in the image sample sets.

5.2. Axial bulk temperature profiles

Figure 2, which gives a schematic representation of the test section, indicates the relative positions of the 11 equally space thermocouple stations on the measuring rod (j = 0 to 10) along the length of the heat exchanger. Consider for a moment the axial position at measuring station j. The inner fluid temperature in the centre of the inner annular space (which was obtained from the thermocouples in the measuring station) is represented by

$T_{i,j}$, while the outer annular bulk fluid temperature at that location is represented by $T_{o,j}$. The wetted wall temperature is represented by $T_{w,j}$, which is used later for the heat transfer coefficient calculations.

Figure 8 gives an example set of the obtained quasi steady-state temperature profiles of the inner fluid for the different heated and annular cases. It can be seen that the temperature profiles were not linear and that a larger temperature gradient was present towards the inlet of the annulus (located at axial position x = 0 mm). This indicates that a higher heat transfer rate was present closer towards the annulus inlet, as expected. Further, it can be seen that as the annular Reynolds number was increased (CA 1 to CA 5 and HA 1 to HA 4), the inner fluid gradient became steeper indicating an overall higher heat transfer rate.

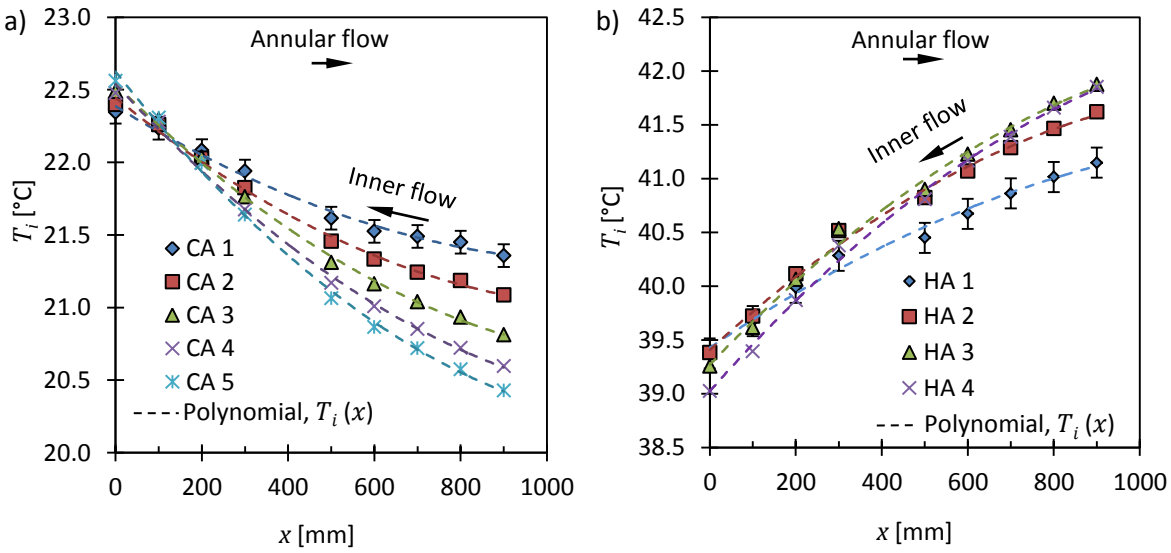

Figure 8 Measuring rod temperatures for a) cooled cases b) heated cases.

The axial locations of the measuring stations where at intervals of 100 mm and did not match with that of the imaging rings which were at intervals of 40 mm. This complicated the heat transfer coefficient calculation which required bulk fluid and wall temperatures at the same axial location. For this reason, second order polynomial fits, $T_i(x)$, were used to

represent the inner fluid axial temperature profiles (also given in Figure 8). This allowed the local bulk fluid temperature to be determined at any axial position. This also reduced the impact of local measuring uncertainties for a single measuring station on the calculated results.

To determine the local bulk fluid temperature on the annular side, which was needed to determine the annular side heat transfer coefficient, seven virtual control volumes n = 1 to 7 were defined that were aligned with the imaging rings. Each control volume spanned both the inner-and annular fluids. The heat transferred from/to the inner fluid in control volume n could be determined by:

$$\dot{Q}_{i,n} = \dot{m}_i C_{p,i}(T_i(x_n) - T_i(x_{n-1})) \quad (1)$$

Here $\dot{m}_i$ is the inner fluid mass flow rate obtained from the inner fluid mass flow meter, $C_{p,i}$ is the specific heat evaluated at the average inner fluid temperature in the control volume by using the equations proposed by Popiel and Wojtkowiak [26] and x_n is the axial position where control volume n ends, such that $x_n = (n-1)L_{CV}$ with L_{CV} = 40 mm. By employing the energy balance principle, the heat transferred from/to the annular fluid per control volume, $\dot{Q}_{o,n}$, was obtained:

$$\dot{Q}_{o,n} = \dot{Q}_{i,n} = \dot{Q}_n \quad (2)$$

Eqn. (2) can be expanded using the heat transfer principle of Eqn. (1):

$$\dot{m}_o C_{p,o}\left(T_{o,n} - T_{o,n-1}\right) = \dot{m}_i C_{p,i}(T_i(x_n) - T_i(x_{n-1})) \quad (3)$$

Here $\dot{m}_o$ is the annular fluid mass flow rate obtained from the annular side mass flow meter and $C_{p,o}$ is the specific heat evaluated at the average annular fluid temperature of the control volume. Subscript n refers to position n at axial distance x_n from the annular inlet.

The only unknown in Eqn. (3) was $T_{o,n}$ which is the annular side exit temperature of the control volume, since all preceding annular bulk fluid temperatures may already be expressed in terms of the measured annular inlet fluid temperature, the mass flow rates and the inner bulk fluid temperature profile.

The local heat transfer coefficient for control volume n, h_n, was obtained via:

$$\dot{Q}_n = h_n A\left(\bar{T}_{w,n} - \bar{T}_{o,n}\right) \tag{4}$$

with $\bar{T}_{o,n}$ was the average annular side bulk fluid temperature:

$$\bar{T}_{o,n} = \frac{T_{o,n} + T_{o,n-1}}{2} \tag{5}$$

The average wetted wall temperature $\bar{T}_{w,n}$ was derived from the local circumferential TLC temperature field, $T_{TLC}(\phi, x)$, and the temperature difference over the resin layer:

$$\bar{T}_{w,n} = \frac{1}{A}\int_A T_{TLC}(\phi, x)dA + \frac{\dot{Q}_n t_{resin}}{k_{resin} A} \tag{6}$$

Here the area weighted average of $T_{TLC}(\phi, x)$ was used and the inner annular surface area was given by $A = \pi D_1 L_{CV}$.

The last term in Eqn. (6) accounts for the temperature difference over the resin layer (with thicknesst_{resin}) due to its low thermal conductivity. Since the resin layer was applied very thinly, a linear, one-dimensional approximation was used for this temperature difference.

The local Nusselt number was then determined as:

$$Nu_o = \frac{h_o D_{h,o}}{k_o} \tag{7}$$

For the calculation of the local overall heat transfer coefficients, the measuring stations (j = 0 to 10) set out by the measuring rod was used since TLC measurements was not required. These coefficients were calculated using the following formula:

$$\dot{Q}_J = U_j A \Delta T_{LMTD} \tag{8}$$

By rearranging and expanding this equation the following was obtained:

$$U_j = \frac{\dot{Q}_j}{A\left(\frac{\left(T_{o,j-1}-T_{i,j-1}\right)-\left(T_{o,j}-T_{i,j}\right)}{\ln\left(\frac{T_{o,j-1}-T_{i,j-1}}{T_{o,j}-T_{i,j}}\right)}\right)} \tag{9}$$

Here Q_j is the heat transfer rate from station $j-1$ to j and was calculated on a similar basis as in Eqn. (1). The inner bulk fluid temperature was based on the appropriate polynomial fit and the annular bulk fluid temperature was calculated using Eqn. (3). Eqn. (9) was applied for separate control volumes to obtain U_j and to the whole heat exchanger to obtain U by using the measured inlet and outlet temperatures of the full test section.

The Reynolds number in the annulus was determined by measuring the mass flow rate of the fluid. The Reynolds number in the annulus was calculated using:

$$Re_o = \frac{\dot{m}_o D_{h,o}}{A_o \mu_o} \tag{10}$$

and the kinematic viscosity of the water was determined at the mean annulus fluid temperature.

5.3 Quasi steady state

As mentioned earlier, it was challenging to maintain strict steady state conditions for the full duration of each test case. Figure 9 supplies a sample of the logged inlet temperatures for the annular and inner fluid for test case CA 1. Even though the inlet temperatures were carefully controlled, small fluctuations did occur. For that reason it was important to consider the impact that small variation in the operating conditions might have had. To compensate for this, the data for each imaging ring (n = 1 to 7) were analysed individually based on its own temporal steady state. Figure 9 show vertical lines which represent the duration and timing for sampling each of the separate ring's images. Any variation in the inlet temperature of the annular- or inner fluid was accounted for by upward or downward translation, and by making use of an updated polynomial fit for the inner bulk fluid temperature profile. This ensured that relevant fluid temperature data was available at each moment when a particular ring was imaged. Once local fluid and TLC temperatures were updated in the time domain and correctly translated, results could be combined for each test case.

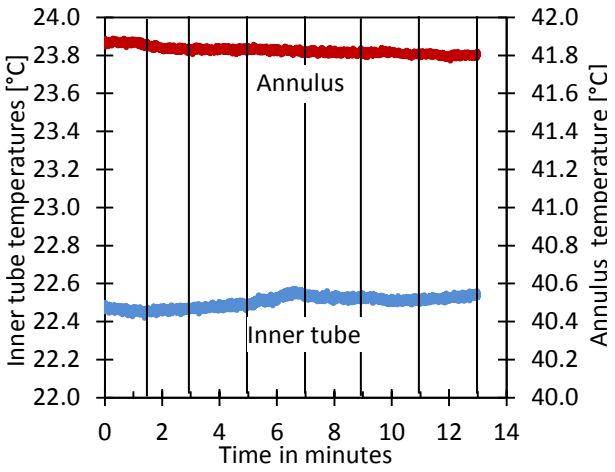

Figure 9 Sample of annular and inner fluid inlet temperatures over time with timing of rings with a 10 Hz sampling rate.

6. Uncertainty analysis

The method for calculating uncertainties used in this study is as described by Kline and McClintock [27]. Shown in Table 3 are uncertainties of some entities which were not affected by the mass flow rates in the annulus.

Table 3 Uncertainties for common entities.

Entity	Uncertainty
δT_i (from polynomial fit)	± 0.023°C, depending on fit
$\delta \Delta T_{CV}$	± 0.033°C, depending on fit
δT_{TLC} (single pixel)	± 0.53°C
$\delta \bar{T}_{TLC}$ (averaged)	± 0.03°C
$\delta T_{i,in}$ and $\delta T_{o,in}$	± 0.05°C
$\delta \Delta T_{o,j}$	± 0.18°C
δk_{resin}	± 2 %

It was found that a relatively high uncertainty of 0.53°C existed for a single TLC extracted pixel. This is due to the manufactured specified uncertainty of 0.22°C, the PT 100 used to calibrate against having an uncertainty of 0.01°C and the maximum deviation from the six order polynomial curve fit shown in Figure 6. This is in line with uncertainty values quoted in literature of between 0.4 °C and 0.5 °C for TLC with a high bandwidth [14, 16]. However, due to the sheer number of pixels (based on 600 clusters) used in calculating the average surface temperature for one of the rings; the effective uncertainty was smaller and found to be approximately 0.03 °C.

Table 4 contains the uncertainty of some calculated quantities, where the annular mass flow rate plays a role on the effective uncertainty. It was found that the uncertainty on the

calculated heat transfer rate per control volume (n = 1 to 7) reduced as the annular mass flow rate increased (CA 1 to CA 5 and HA 1 to HA4), but that the uncertainty on the heat transfer coefficient increased.

Table 4 Uncertainties on calculated values.

	Cooled annular cases					Heated annular cases			
Case	CA 1	CA 2	CA 3	CA 4	CA 5	HA 1	HA 2	HA 3	HA 4
$\delta\dot{Q}_n$ [%]	49	38	32	29	26	36	28	24	22
$\delta\Delta T_{resin}$ [°C]	3.1	3.1	3.1	3.1	3.2	2.2	2.2	2.2	2.2
δh_n [%]	57	54	60	87	123	45	40	43	46
δU [%]	6	9	4	3	3	7	4	3	3

The relatively large uncertainties for the local heat transfer coefficients were due to the relatively small change of axial bulk fluid temperature which increased the uncertainty of the local heat transfer rate, but also due to the small difference between the fluid bulk temperature and the wetted wall temperature on the annular side. Although the uncertainty of the local temperature inner fluid bulk temperature was low ($\delta T_{i,j}$ = 0.078°C), the temperature change over a control volume was relatively small and was as low as 0.11°C when the annular flow rate was low. By increasing the control volume length, the uncertainty values can be reduced, as illustrated in Table 5. For instance, by increasing the control volume length, L_{CV}, from 40 mm to 120 mm for case CA 1 ($\mathrm{Re}_o \approx 1\,000$), the local heat transfer uncertainty can be reduced from 57% to 12%.

Table 5 Influence of control volume length on the uncertainty of $\boldsymbol{h_n}$.

	Cooled annular cases					Heated annular cases			
Length of control volume, L_{CV}	CA 1	CA 2	CA 3	CA 4	CA 5	HA 1	HA 2	HA 3	HA 4
40 mm	57 %	54 %	60 %	87%	123%	45%	40%	43%	46%
80 mm	18%	21%	25%	32%	50%	14%	17%	21%	25%
120 mm	12%	12%	15%	23%	18%	11%	11%	14%	16%
280 mm	6%	8%	11%	16%	18%	5%	7%	10%	12%

7. Results

7.1 TLC temperature field

Table 6 gives two example sets of the extracted TLC temperatures $T_{TLC}(\phi, x)$ for cases CA 3 and HA 3 ($\mathrm{Re}_o \approx 5\,000$). It can be seen that there was a wide variation in the measured TLC temperatures, which would have been difficult to obtain from thermocouple measurements. Ring 1 and 2 (n = 1 and 2) were partially recorded covering a circumferential range of 252° due to physical interference between the camera mechanism and the inlet port to the annulus. It was found that a temperature variations of up to 8.1 °C and 3.5 °C for cases CA 3 and HA 3 respectively existed between the warmest and coldest positions on the inner annular wall within the first 300 mm of the annular inlet. The measurements show that the temperature distributions obtained from LCT were relatively symmetrical around the circumference of the inner annular wall. All cases (heated and cooled respectively) exhibited similar temperature distributions. For a cooled annulus, which received warm water perpendicularly from above at ϕ = 0° and x = 0 mm, it appears as if the hot water swept around the inner tube of the annulus and impinged the annular wall from below at

Table 6 Extracted temperatures [°C] from TLC's at inlet (darker means warmer).

		Cooled annulus CA 3								Heated annulus HA 3						
n:		1	2	3	4	5	6	7		1	2	3	4	5	6	7
$\bar{x}$ [28]:		20	60	100	140	180	220	260		20	60	100	140	180	220	260
ϕ	-180°	27.5	27.1	25.8	30.3	29.1	29.5	27.7		35.6	35.7	35.9	35.4	35.8	35	35.2
	-144°	27.5	25.1	25.2	29.4	28.3	27.7	27		35.8	35.5	36	34.2	35.5	33.2	33.2
	-108°	27.4	25	24.7	28.7	27.3	27.5	27.1		35.9	35.7	36.1	35.7	36.3	35	35.2
	-72°	27.5	25.1	24.7	28.1	26.2	26.3	25.9		36.2	35.9	36.5	36	36.6	35.8	35.7
	-36°			25.2	27.2	25.8	25.1	25.4				36.6	36.3	36.7	36.1	36
	0°			25.1	27.2	25.8	25.3	25.3				36.7	36.4	36.7	36.1	36.2
	36°			24.6	27.2	26	25.9	25.4				36.5	36.4	36.7	36.1	36.2
	72°	27.3	25.3	24.3	28	27	27.1	26.3		36.1	35.9	36.3	36.3	36.7	35.9	35.1
	108°	27.3	24.9	24.8	30.4	28.5	29.3	27.9		35.8	34.8	36	36.3	36.4	35.9	35.7
	144°	27.5	25.3	24.9	32.4	30.9	30.9	29.7		35.6	35.7	35.4	35.9	36.2	35.6	35.7

	180°	27.5	27.1	25.8	30.3	29.1	29.5	27.7		35.6	35.7	35.9	35.4	35.8	35	35.2

approximately $\phi \approx 180°$ and $x \approx 140$ mm, where the highest wall temperature was situated. The upper regions ($\phi \approx 0°$) of the inner annular wall were relatively cold. Similarly for the heated annular cases, which received cold water, it appears as if the cold water impinges the inner annular wall from below ($\phi \approx 180°$), and that the upper regions were warmer. Unfortunately, the region directly in line with the annular inlet ($\phi = 0°$ and $x = 0$ mm) could not be imaged, and it is anticipated that the most extreme impingement occurs there for both heated and cooled cases.

7.2 Heat transfer coefficients

The circumferentially averaged TLC temperaures were determined for each imaging ring (n = 1 to 7). After applying Eqns. (3), (5) and (6) the local inner and annular bulk fluid temperatures and the local wetted inner annular surface temperatures were determined. Figure 10 and Figure 11 show these temperature trends for cases CA 1 and CA 5 respectively. The data for n = 1 and 2 are also included here, but it should be kept in mind that these rings were only partially mapped thermographically. It can be seen that the thermal resistance of the resin had a significant effect, even when the resin layer was thin. Thus, care had to be taken when measuring the thermal conductivity of the resin. It could be noted that there was a disturbance in the wall temperature at about 140 mm from the inlet. This occurred for all cooled cases and is linked to the TLC temperature profiles. This behaviour was not noticed for the heated annular cases. The variation in the local wall temperature is indicative of a fluctuation in the local heat transfer rate and/or an

improvement in the mixing phenomenon and thus a higher heat transfer coefficient influenced by the inlet flow velocity distribution.

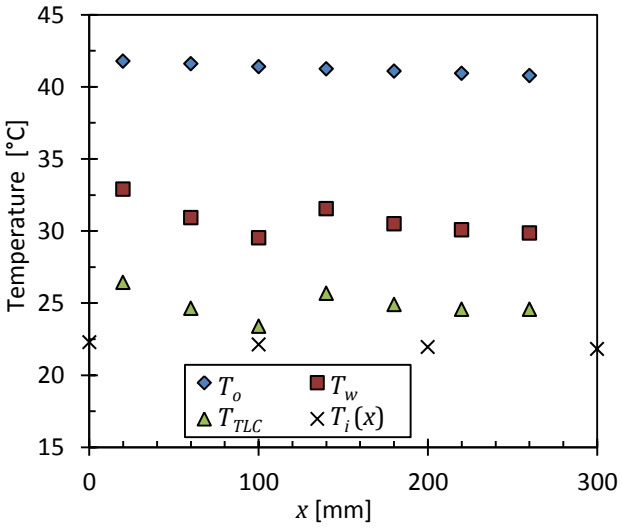

Figure 10 Wall and bulk temperatures for CA 1.

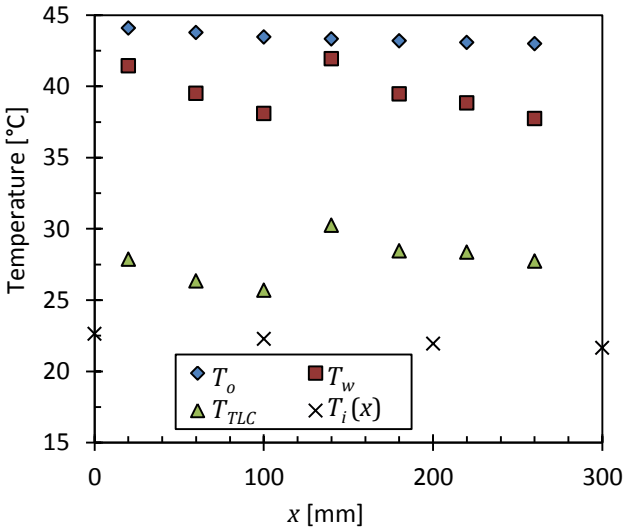

Figure 11 Wall and bulk temperatures for CA 5.

Figure 12 and Figure 13 show the calculated annular local heat transfer coefficients for all the cooled and heated test cases respectively. For clarity reasons a logarithmic scale for the heat transfer coefficient is used. For the cooled cases it can be seen that the heat transfer coefficients varied significantly along the tested length and that the peak heat transfer

coefficient was found to occur at 140 mm from the inlet of the annulus. This is directly linked to the temperature disturbance on the annulus wall. The heated annular cases showed less variation and the highest heat transfer coefficients appears to be directly in line with the annular inlet and decreased towards the exit of the annulus.

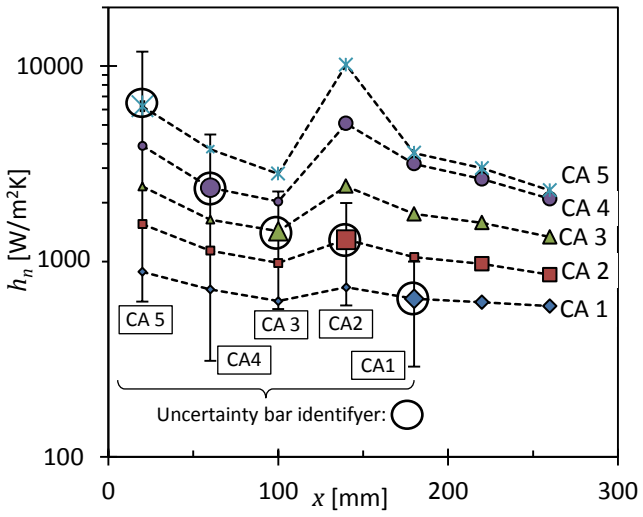

Figure 12 Local heat transfer coefficients for the cooled annular cases.

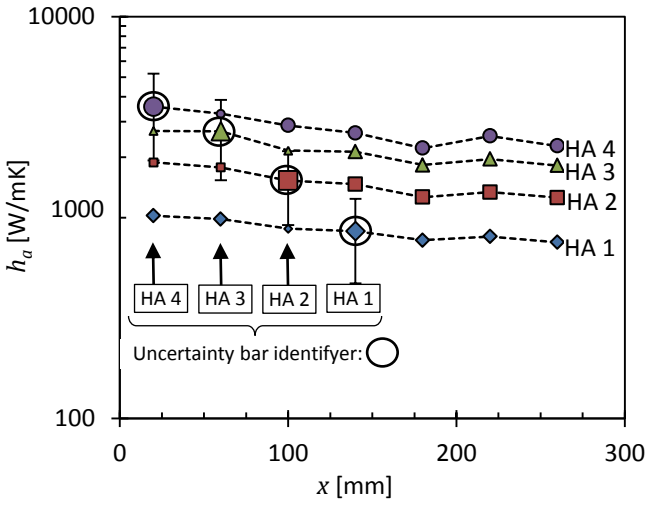

Figure 13 Local heat transfer coefficients for the heated annular cases.

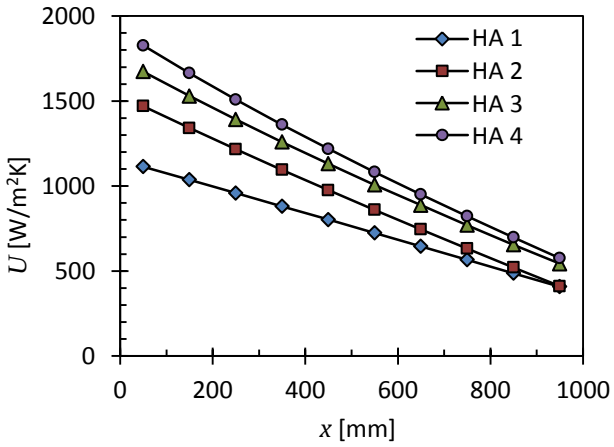

Figure 14 Overall heat transfer coefficients along the length of the heat exchanger (heated annulus).

The local overall heat transfer coefficient as calculated by Eqn. (9) is shown in Figure 14. The values of U_j only rely on the bulk fluid temperature change as measured by the inner measuring rod. Figure 14 shows the overall heat transfer coefficient distribution along the length of the heat exchanger. It clearly shows that the heat transfer potential is higher at the annular inlet of the heat exchanger and reduces as one move along the length. The relative behaviour of U for cases HA1 to HA4 also mimics the relative behaviour of h_a shown in Figure 13.

Table 7 Averaged values for experimental data.

	Cooled annular cases					Heated annular cases			
	CA 1	CA 2	CA 3	CA 4	CA 5	HA 1	HA 2	HA 3	HA 4
Re_o	1 000	2 500	5 000	10 000	13 600	1 000	2 500	5 000	8 000
eb	1.0	0.4	1.4	2.7	6.5	0.3	2.8	5.6	8.9
$\bar{h}_{o,inlet}$	759	1232	2000	3509	5683	675	1188	1733	2176
$\overline{Nu}_{o,inlet}$	17.1	27.7	44.9	80.6	127.6	15.9	27.1	41.0	51.5
$\bar{U}_{overall}$	321	375	450	521	539	292	349	399	415

Table 7 gives a summary of the arithmetic averaged local heat transfer coefficient values (convective and overall) as well as the Nusselt numbers for the investigated inlet region across n = 1 to 7. Also given are the energy balances achieved for each test case over the entire length of the heat exchanger. The energy balance is defined as the percentage difference in heat transfer rate between the annular cavity and the average of the annular and the inner cavity:

$$eb = \left(\dot{Q}_o - \frac{\dot{Q}_o+\dot{Q}_i}{2}\right) / \left(\frac{\dot{Q}_o+\dot{Q}_i}{2}\right) \times 100\% \quad (11)$$

For the cooled annular cases energy balance errors of less than 3% were achieved for Reynolds numbers between 1000 to 10 000. For heated annular cases energy balance errors of less than 3% were only obtained for Reynolds numbers between 1000 and 2500. Higher mass flow rate cases were associated with poorer energy balances, which are attributed to smaller measured temperature differences from the inlet to the outlet of the annulus. This is a direct result of the relatively short heat exchanger considered in the study.

7.3 Comparison with existing correlations

The heat transfer values (in the turbulent flow regime) will now be compared with the results obtained using the existing correlations outlined in Table 1. The included correlations were chosen carefully. In order to compare the data obtained in this study with existing literature, it was checked whether the correlations in questions were obtained or derived from data for similar operating conditions. This mostly relates to data based on the same Reynolds numbers in the annulus and the annular diameter ratio which was equal to 0.54 as was the case in the present study. It must, however, be noted that some correlations were derived from data taken from heat exchangers up to 5 m in length and were designed to

supply only overall performance measures (in terms of the averaged Nusselt number). The impact of the length of the heat exchanger relative to the respective diameters (length to diameter ratio) must also be considered. In most of the literature sources little emphasis is placed on this as is evident from the absence of length-based terms or coefficients within the equations. For this reason, and because of the limited number of operating data points available at present, it is not possible to make a recommendation regarding the suitability of a single correlation. The only correlation with a term for the heat exchanger length is that of Gnielinski [5]. For comparative purposes the correlation was applied to hypothetical heat exchanger lengths of 280 mm and 1 m representing the control volume length under consideration now, as well as the full heat exchanger length.

The arithmetic averaged Nusselt number values as presented in Table 7, as well as the Nusselt numbers that were obtained using a single 280 mm long control volume are plotted against the predictions from the correlations these correlations in Figure 15 and Figure 16 for the cooled and heated cases respectively. It should be noted that the Nusselt numbers calculated from the single 280 mm long control volume had Nusselt numbers higher than the arithmetic averaged Nusselt numbers. Both are included here.

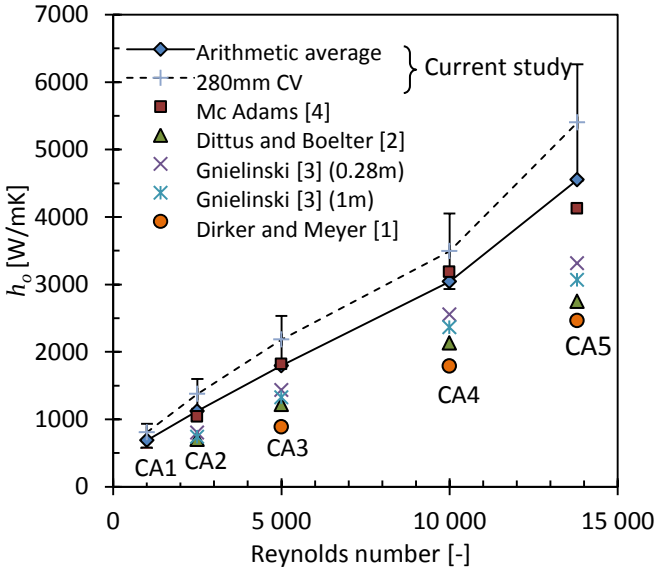

Figure 15 Comparison with existing correlations (cooled annulus).

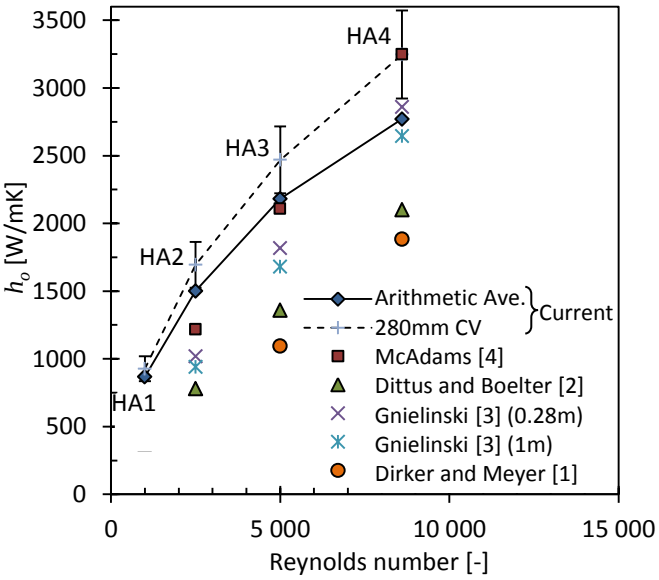

Figure 16 Comparison with existing correlations (heated annulus).

Of the correlations under consideration, the one by McAdams [4] predicted the highest heat transfer coefficients and were in closest agreement with the results of this study, being within 5% from the arithmetic averaged experimental Nusselt numbers for cases CA2 to CA4 and within 10% for case CA5. (Case CA1 is in the laminar flow regime). For heated cases HA2 to HA4 it gave predictions with 20% from the experimental values. The rest of the

correlations predicted lower values but their predictions were relatively close to one another within a band of about 20% based on their average.

Since the data presented relates only to the inlet region, it is reasonable to suggest that the higher experimentally obtained results are due to higher heat transfer rates at the inlet region for developing flow. The prediction by the correlation by Gnielinski [5] for a heat exchanger of a shorter length (0.28 m) did produce a slightly higher Nusselt number than for the whole (1 m long) heat exchanger, but only marginally. This shows that this correlation does account somewhat for entrance effects, but that it was not able to predict the higher inlet effect sensitivity in the experimental values.

As some literature sources suggests, the direction of heat transfer also has an effect on the heat transfer coefficients. In general it is expected that the heat transfer coefficients are higher for heated cases [2, 7]. This was also reflected in the current experimental results as is evident when comparing the cooled and heated cases in Figure 15 and Figure 16.

Based on the data points included here it is possible to estimate the Reynolds number exponent that might be useful to predict the experimentally obtained heat transfer coefficients. If a Dittus-Boelter type correlation [2] is considered using a coefficient of 0.023, the Reynolds number exponent appears to be in the range of 0.8187 and 0.8467, while for a McAdams type correlation [4] using a coefficient of 0.03105, the Reynolds number exponent was found to be in the range of 0.8027 and 0.8054. In order to fully determine the correlation coefficients and the Reynolds number exponents, a larger experimental data set is needed, which falls beyond the scope of this article. Alternative inlet configurations could also be investigated by implementing LCT.

8. Conclusion

Liquid Crystal Thermography (LCT) was successfully implemented as a wall temperature measurement technique for a tube-in-tube heat exchanger. A methodology was developed with which the wall temperatures could be determined without using thermocouples in a water-operated heat exchanger. It was found that TLC has sufficient temperature response with which local temperature distributions may be determined. The obtained temperature fields also showed large temperature variations close to the inlet of the heat exchanger, which may be problematic when using low sampling average wall temperature measurement techniques such thermocouples. The wall temperature uncertainties were found to be very low (±0.03°C for $\bar{T}_w$), which indicated that LCT could be an invaluable tool for measuring wall temperatures.

The measured temperature distributions were used to calculate local heat transfer coefficients which related well with some currently available literature. The experimental heat transfer coefficients were, however, found to be higher than the predictions by the majority of the other correlations considered. This is probably due to a developing boundary layer present near the inlet of the heat exchanger.

9. Recommendations / Further work

As more heat transfer data becomes available from using the current method, it is recommended that heat transfer coefficient correlations be developed for heat exchangers that are dominated by inlet region effects. It is also recommended that experimental uncertainty relating to the heat transfer rate could be reduced by implementing a constant heat flux at the inner wall of the annulus.

Acknowledgements:

The Funding obtained from the NRF, TESP, University of Stellenbosch/ University of Pretoria, SANERI/SANDENI, CSIR, EEDSM Hub and NAC is acknowledged and duly appreciated.

Bibliography

[1] J. Dirker and J. P. Meyer, "Convective heat transfer coefficients in concentric annuli", *Experimental heat and mass transfer,* vol. 17, pp. 19-29, 2005.

[2] F. W. Dittus and L. M. K. Boelter, *Publications on engineering,* vol. 2, p. 443, 1930.

[3] V. Gnielinski, "New equations for heat and mass transfer in the turbulent flow in pipes and channels", *International chemical engineering,* vol. 16, pp. 359-368, 1975.

[4] W. H. McAdams, *Heat transmissions*, 3rd ed. New York, 1954.

[5] V. Gnielinski, "Heat transfer coefficients for turbulent flow in concentric annular ducts", *Heat transfer engineering,* vol. 30, pp. 431-436, 2009.

[6] A. N. Smith and H. Nochetto, "Laminar thermally developing flow in rectangular channels and parallel plates: uniform heat flux", *Heat mass transfer,* vol. 50, 2014.

[7] W. R. v. Zyl, J. Dirker, and J. P. Meyer, "Single-phase convective heat transfer and pressure drop coefficients in concentric annuli", *Heat transfer engineering,* vol. 34, pp. 1112-1123, 2013.

[8] Y. A. Cengel, *Heat and mass transfer*, Third ed. New York: Mc Graw Hill, 2006.

[9] G. Maranzana, I. Perry, and D. Maillet, "Mini- and micro-channels: influence of axial conduction in the walls", *International journal of heat and mass transfer,* vol. 47, 2004.

[10] M. Mirzaei, M. Saffar-Avval, and H. Naderan, "Heat transfer investigation of laminar developing flow of nanofluids in a microchannel based on eulerian-lagrangian

approach", *The Canadian journal of chemical engineering,* vol. 92, pp. 1139 - 1149, 2014.

[11] S. N. Singh, "Heat transfer by laminar flow in a cylindrical tube", *Applied sciences,* vol. 7, 1957.

[12] B. Shiniyan, R. Hosseini, and H. Naderan, "The effect of geometric parameters on mixed convection in an inclined eccentric annulus", *International journal of thermal science,* vol. 68, pp. 136-147, 2013.

[13] A. J. Ghajar and L. M. Tam, "Heat transfer measurments and correlations in the transition region for a circular tube with three different inlet configurations", *Experimental thermal and fluid science,* vol. 8, pp. 79-90, 1994.

[14] Y. Rao and S. Zang, "Calibration and the measurement uncertainty of wide-band liquid crystal thermography ", *Measurement science and technology,* vol. 21, 2010.

[15] C. Camci, *Color recognition for temperature measurements on liquid crystal coated heat transfer surfaces*.

[16] Y. Rao and Y. Xu, "Liquid crystal thermography measurement uncertainty analysis and its application heat transfer measurements", *Advances in condensed matter physics,* vol. 2012, 2012.

[17] H. H. Al-Ali and M. S. Selim, "Momentum and heat transfer in the entrance region of a parallel plate channel: developing laminar flow with constant wall temperature", *Applied scientific research,* vol. 51, pp. 663-675, 1993.

[18] R. E. Critoph, M. K. Holland, and M. Fisher, "Comparison of steady state and transient methods for measurement of local heat transfer in plate fin-tube heat exchangers using liquid crystal thermography with radiant heating", *International journal of heat and mass transfer,* vol. 42, pp. 1-12, 1999.

[19] T. R. Ogden and E. W. Hendricks, "Liquid crystal thermography in water tunnels", *Experiments in fluids,* vol. 2, pp. 65-66, 1984.

[20] M. K. Chyu, H. Ding, J. P. Downs, and F. O. Soechting, "Determination of local heat transfer coefficient based on bulk mean temperature using a transient liquid crystal technique", *Experimental thermal and fluid science,* vol. 18, 1998.

[21] J. Stasiek, M. Ciofalo, and M. Wierzbowski, "Experimental and numerical simulations of flow and heat transfer in heat exchanger elements using liquid crystal thermography", *Journal of thermal science,* vol. 13, pp. 133-137, 2044.

[22] H. Li, C. Xing, and M. J. Braun, "Natural convection in a bottom-heated top-cooled cubic cavity with a baffle at the median height: experiment and model validation", *Heat mass transfer,* vol. 43, pp. 895-905, 2007.

[23] C. Camci, *Introduction to liquid crystal thermography and a brief review of past studies*.

[24] T. Moeslund, *Introduction to video and image processing*. New York: Springer, 2012.

[25] P. M. K. Jr and J. K. Eaton, "Angular effects on thermochromic liquid crystal thermography", *Experimental fluids,* vol. 43, pp. 929-937, 2007.

[26] C. O. Popiel and J. Wojtkowiak, "Simple formulas for thermophysical properties of liquid water for heat transfer calculations", *Heat transfer engineering,* vol. 19, pp. 87-101, 1998.

[27] S. Kline and F. McClintock, "Describing uncertainties in single-sample experiments", *Mechanical engineering,* vol. 75, pp. 2-8, 1969.

[28] ACEoT Measurement, *Manual on the use of thermocouples in temperature measurement*, 4th ed.: ASTM International, 1993.

Nomenclature

A	m^2	area
a	-	ratio between annulus and inner diameter
C_p	J/kg.K	specific heat
C	-	Dirker and Meyer correlation coefficient
CV	-	control volume
D	m	diameter
D_h	m	hydraulic diameter
eb	%	energy balance
f	-	friction coefficient
G_1 - G_4	-	Gnielinski correlation factors
HSV	°,-,-	Hue, Saturation, Value colour
h	W/m^2K	heat transfer coefficient
k	W/mK	thermal conductivity
L	m	total heat exchanger length
L_{CV}	m	length of control volume
m	-	exponent
$\dot{m}$	kg/s	mass flow rate
Nu	-	Nusselt number
P	-	coefficient in Dirker and Meyer correlation
Pr	-	Prandlt number
$\dot{Q}$	W	heat transfer rate

RGB	-	Red, Green, Blue colour system
Re	-	Reynolds number
Re^*	-	modified Reynolds number
t_{resin}	m	resin layer thickness
T	°C	temperature
$\bar{T}$	°C	average temperature
U	W/mK	Overall heat transfer coefficient
x	m	axial position
Greek symbols:		
Δ	-	change in entity
δ	%	uncertainty
μ	m^2/s	kinematic viscosity
ρ	kg/m^3	density
ϕ	rad or °	angular position
Subscripts:		
ave		average property
b		bulk property
CV		control volume
h		based on hydraulic diameter
i		inner tube
in		inlet
j		measuring rod control volume index number

LMTD		Local mean temperature difference
local		local property
n		imaging ring control volume index number
o		Annulus side
out		outlet
resin		resin layer
TLC		Thermochromic Liquid Crystal
w		inner tube outer wall